Check for updates

Electronics Letters

LETTER OPEN ACCESS

Digital Predistortion of Power Amplifiers for Quantum Computing

Marvin Jaeger | Bartosz Tegowski | Georg Frederik Riemschneider | Alexander Koelpin

Institute of High-Frequency Technology, Hamburg University of Technology, Hamburg, Germany

Correspondence: Marvin Jaeger (marvin.jaeger@tuhh.de)

Received: 28 April 2026 | **Revised:** 4 August 2026 | **Accepted:** 19 August 2026

ABSTRACT

Power amplifiers (PA) are essential for microwave-controlled trapped-ion and semiconductor spin based quantum computers (QC). They adjust the power level of the control signal and therefore the processing time of the QC. Their nonlinearities and memory effects degrade the signal quality and, thus, the fidelity of qubit gate operations. Driving the PA with a significant input power back-off reduces nonlinear effects but is neither power-efficient nor cost-effective. To overcome this limitation, this letter augments the conventional signal generation system applied in QCs by digital predistortion (DPD) to linearize the radio frequency (RF) channel. Numerical analysis of the qubit behavior based on measured representative control signals indicates that DPD improves its fidelity.

1 | Introduction

Quantum computers (QC) are predicted to be superior to classical computers in solving probability-based problems. Unlike classical computers, which use the distinct states "0" and "1", QCs use the superposition of the quantum states $|0\rangle$ and $|1\rangle$, which forms the qubit state. There exist different physical implementations of qubits, such as superconducting qubits, trapped ions, and semiconductor spin qubits, whose quantum states can be manipulated by using microwave control signals [1, 2]. Therefore, the quality of the microwave control signals directly affects the qubit state fidelity of quantum operation [3]. The signal quality depends on the signal generation system, where the power amplifier (PA) ensures a sufficient output power level. The PA; however, is a nonlinear device with memory elements, which leads to amplitude errors, time delay, phase shifts, and spurious generation, thereby decreasing the fidelity. In quantum computing, a common method to compensate for those nonideal effects is to increase the input power back-off (IBO), which requires PAs with higher output powers to maintain a specified power level to drive the qubit gates. This increases costs and decreases power efficiency.

Instead of increasing the IBO, the nonlinearities and memory effects can be compensated. Early linearization relied on analog feedforward and feedback techniques. However, with today's high bandwidths and adaptation requirements, digital predistortion (DPD) has become established in communication engineering [4], while analog predistortion [5] represents a viable alternative that can provide wideband linearization at high carrier frequencies with inherently low latency, albeit with reduced flexibility for reconfiguration. In DPD, the inverse of the nonlinear transfer function is modeled in the digital domain and applied to the input signal to linearize the overall system. Commonly used regression-based methods are the generalized memory polynomial (GMP) [6] and its parameter-reduced form, that is, the memory polynomial (MP) [7]. Different neural-network-based DPD approaches have also been reported in the literature, employing feedforward networks [8], residual recurrent neural networks (RNNs) [9], and reinforcement-learning-based coefficient adaptation [10].

This is an open access article under the terms of the Creative Commons Attribution License, which permits use, distribution and reproduction in any medium, provided the original work is properly cited.
© 2026 The Author(s). *Electronics Letters* published by John Wiley & Sons Ltd on behalf of The Institution of Engineering and Technology.

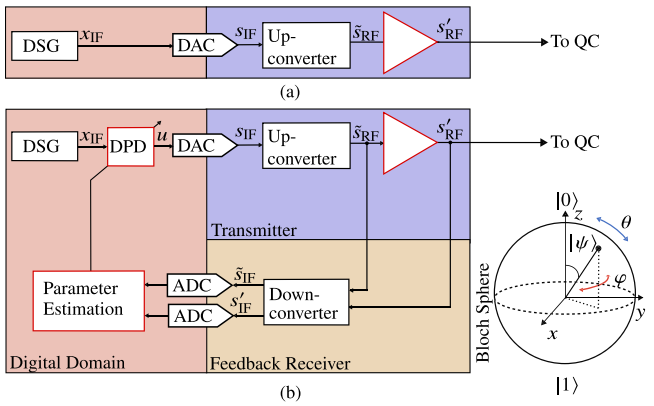


FIGURE 1 | Conceptual transmitter architecture of (a) a classical quantum control system and (b) a quantum control system extended by DPD and a feedback loop for PA characterization. The Bloch sphere visualizes the qubit state $|\psi\rangle$.

All linearization methods involve a tradeoff between computational complexity and the achievable performance of the power amplifier (PA), in terms of power efficiency and linearity.

In quantum-control systems, signals are either precomputed and replayed using an arbitrary waveform generator [11] or real-time calculated based on given waveform parameters [12]. Computational complexity and processing latency are relevant for live waveform generation but do not affect relative gate timing. Achieving accurate wideband DPD requires sufficient bandwidth in the digital-to-analog converters (DACs), analog-to-digital converters (ADCs), and frequency-conversion stages. Existing quantum-control signal generators, such as the QICK platform [12], already consist of high-performance components, enabling the integration of DPD with only limited additional system adaptation.

This letter studies the application of DPD to the control signal generation dedicated for microwave-controlled QCs. For this, the classical transmitter architecture [12, 13], shown in Figure 1a, is augmented by a feedback receiver and DPD functionality as indicated in Figure 1b. By compensating for the nonlinearities and memory effects of the PA, the control signal accuracy can be improved. Numerical simulations of qubit state evolution based on measured control signals indicate an improvement in fidelity without compromising the output power. In quantum-control systems, linear equalization, pulse shaping, and error-compensating control pulses are widely used and actively researched [11]. However, to the best of the authors' knowledge, the explicit application of DPD to quantum control signal generation and the evaluation of its performance in terms of qubit state fidelity has not yet been reported.

2 | Qubit Gate Operation

In a QC, a single qubit state can be expressed as [2, eq. (1)]

$$|\psi\rangle = \alpha|0\rangle + \beta|1\rangle, \tag{1}$$

where α and β are complex-valued probability amplitudes normalized by $|\alpha|^2 + |\beta|^2 = 1$. It can be represented in the Bloch sphere with the corresponding angles θ and φ, as depicted in Figure 1b. A defined rotation in θ and φ forms a qubit gate operation, represented by the state evolution matrix U, which changes the initial qubit state $|\psi\rangle$ to the final state [14, eq. (7.2)]

$$|\psi'\rangle = U \cdot |\psi\rangle. \tag{2}$$

The qubit gate can be numerically approximated by [3, eq. (1)]

$$U \approx \prod_{n=N}^{0} \exp\left(-jH(n\Delta t)\Delta t\right), \tag{3}$$

where H denotes the Hamiltonian, n the discrete time index, Δt the time step, and $\exp(\cdot)$ the matrix exponential. Equation (3) approximates the time-varying Hamiltonian by a product of time-independent components. For single-qubit gate operation, the Hamiltonian in the rotating frame under the rotating wave approximation is defined as [11, eq. (91)]

$$H(n\Delta t) = -\frac{\Omega_R}{2}\left(\Re\{s_{BB}(n\Delta t)\}\sigma_x + \Im\{s_{BB}(n\Delta t)\}\sigma_y\right), \tag{4}$$

where σ_x and σ_y are the Pauli matrices and $s_{BB}(t)$ is the equivalent baseband representation of the microwave qubit excitation signal. A sufficiently small time step Δt is required to ensure an accurate numerical approximation of the Hamiltonian.

The qubit state fidelity [15, eq. (1)]

$$F = |\langle\psi_{ideal} \mid \psi\rangle|^2 \tag{5}$$

evaluates how close the qubit state $|\psi\rangle$ is to the ideal gate $|\psi_{ideal}\rangle$.

3 | Quantum Control Signal Generation

For qubit implementations based on trapped-ions or semiconductor spin qubit types considered in this work, the qubit state can be adjusted by a microwave signal whose frequency corresponds to the qubit excitation frequency f_e. The signal amplitude is proportional to the Rabi frequency Ω_R, which is the angular speed of rotation along θ and mainly impacts the QC processing speed. The phase of the signal controls the angle φ. Simultaneous processing of multiple qubits can be realized by spatial or frequency multiplexing. For example, this is exploited by the magnetic gradient induced coupling (MAGIC) principle [16].

To excite N frequency multiplexed qubits for M_n consecutive gates, the multitone signal

$$s'_{RF}(t) = \sum_{n=0}^{N-1} s'_{RF,n}(t) \tag{6}$$

is applied, following a pulsed frequency-division multiplexing (FDM) scheme, where each tone

$$s'_{RF,n}(t) = \sum_{m=0}^{M_n-1} \Re\left\{s_{BBm,n}(t) \cdot e^{j2\pi f_{e,n} t}\right\} \tag{7}$$

1350911x, 2026, 1, Downloaded from https://ietresearch.onlinelibrary.wiley.com/doi/10.1049/el2.70708 by Technische Universität Hamburg Universitätsbibliothek, Wiley Online Library on [14/09/2026]. See the Terms and Conditions (https://onlinelibrary.wiley.com/terms-and-conditions) on Wiley Online Library for rules of use; OA articles are governed by the applicable Creative Commons License

with

$$s_{\mathrm{BB}m,n}(t) = A_{m,n} \cdot p_{m,n}(t - \tau_{m,n}) e^{j\phi_{m,n}} \tag{8}$$

individually controls its associated qubit, which exhibits the excitation frequency $f_{e,n}$. $A_{m,n}$ denotes the amplitude of the pulse, $\phi_{m,n}$ is the pulse phase, and $p_{m,n}(t)$ is the pulse form applied for each gate at $\tau_{m,n}$ for the mth gate, which can be summarized to the baseband signal $s_{\mathrm{BB}m,n}(t)$. For a rectangular pulse of duration T, the θ-rotation in the Bloch sphere amounts to $\theta = \Omega_R \cdot T \propto A_{m,n} \cdot T$.

Figure 1a shows a typical generation system [12, 13], which intends to output the signal (6). It is generated as the equivalent baseband (BB) signal $s_{BB_{m,n}}$ and upconverted to the intermediate frequency (IF) band signal x_{IF} using a digital signal generator (DSG) in the digital domain. A DAC converts the digital signal into the analog domain. The transmitter transforms this IF signal s_{IF} into the required radio frequency (RF) signal s'_{RF} by upconversion and amplification as in [13]. The RF band is determined by the excitation frequency of the qubits.

Compared to the upconverter, the PA introduces the dominant signal distortion in the transmitter chain, which degrades the signal quality. The characteristics of the PA can be described as

$$s'_{\mathrm{RF}}(t) = G_{\mathrm{lin}} \cdot h\{\tilde{s}_{\mathrm{RF}}(t)\}, \tag{9}$$

where G_{lin} is the linear gain and $h\{\cdot\}$ is the dynamic transfer function, which accounts for nonlinearities and memory effects. The nonlinear effects are due to saturation and lead to amplitude compression (AM/AM) and amplitude-dependent phase distortion (AM/PM). The memory effects can be separated into long-term memory (LTM) and short-term memory (STM) [17]. LTM is caused by thermal effects, supply modulation, trapping, and device aging, while STM is due to parasitic circuit components.

These effects can be mitigated by applying DPD in the digital domain, where the intermediate-frequency signal s_{IF} is predistorted to obtain the output signal u, as shown in Figure 1b. To model the inverse of the PA transfer function $h^{-1}\{\cdot\}$ required for DPD, the classical signal generation system is extended by a measurement of the in- and the output signal of the PA. For this, a feedback receiver is introduced, which downconverts the PA's input and output signals $\tilde{s}_{\mathrm{RF}}$ and s_{RF} to the IF signals $\tilde{s}_{\mathrm{IF}}$ and s'_{IF}, respectively, where they are digitized by an ADC. Using an indirect learning architecture, a parameter estimation algorithm estimates $h^{-1}\{\cdot\}$ and adjusts the DPD, by using, for example, a least squares estimator or other optimization techniques. The achievable DPD performance is limited by the model, its capacity, as well as the accuracy of the feedback path.

4 | Experimental Results

To evaluate the effectiveness of DPD in the context of quantum computing, the qubit gate fidelity is numerically simulated based on measured qubit control signals without and with DPD applied.

4.1 | Experimental Setup

The measurements of representative control signals are performed on the RF WebLab platform [18], which consists of a vector signal transceiver (National Instruments PXIe-5646R) and a gallium nitride PA (Cree CGH40006-TB). Even though the system is not dedicated for the control of a QC, it implements the signal generation system depicted in Figure 1b. Thus, it is representative to study the impairments of the microwave signal quality, the consequences of which can be discussed in terms of QC operation by means of numerical qubit simulations according to (2)–(5). The system has a measured linear gain of 25.48 dB and supports a 200-MHz bandwidth at 2.14-GHz center frequency. The received signal is synchronized by adding a maximum length sequence to the signal, upsampling by a factor of 10, applying a circular cross correlation, and downsampling by the same factor.

To demonstrate the effectiveness of DPD, signals for frequency-multiplexed qubits are used, which strongly suffer from nonlinear effects due to their high dynamic range. As an example, $N = 4$ BB signals are considered, where each one is devoted to one simulated qubit at 2.145, 2.17, 2.19, and 2.215 GHz, leading to a signal bandwidth of approximately 70 MHz, with the overall signal formed by their superposition according to (6). The signal is separated into sequences, each consisting of four frames of equal duration $T = 1.6\ \mu$s. Within each frame, each of the four qubits is independently either driven by a π-pulse or left idle. For every qubit, a sequence consists of two π-pulses and two idle-pulses, ideally implementing an identity operation; 20 subsequent sequences are applied. The order of the pulses within one sequence is randomly selected and individual for each qubit excitation. The π-pulses are randomly chosen between $\pm X_\pi$, and $\pm Y_\pi$, where X and Y denote a rotation around the x- and y-axis in the Bloch sphere, respectively. To suppress image frequencies, a single-sideband (SSB) modulation is applied during the signal generation. The transmitted signal s_{IF} has an overall peak-to-average power ratio (PAPR) of 9 dB, numerically calculated over the full test signal, with a per-tone PAPR of 3 dB resulting from the 50 % duty cycle of each tone's activation and an average output power of $P_n = -22.5$ dBm per tone, which is assigned to a maximum Rabi frequency of $\Omega_{R,\max}$. The baseband signal amplitude spans the full range from no excitation (all qubits idle) to full constructive superposition of all qubits.

As an example among different DPD algorithms, the MP is used, which is defined as [7]

$$u = \sum_{k=1}^{K} \sum_{l=0}^{L-1} a_{k,l}\, x_{\mathrm{IF}}(n-l)\, |x_{\mathrm{IF}}(n-l)|^{k-1}, \tag{10}$$

where $a_{k,l}$ are the coefficients weighting the nonlinear order k and memory depth l, estimated by applying a least-squares estimator to a training data set of 50 consecutive sequences. Compared to the neural-network-based approaches discussed in the introduction, the MP model was chosen for its lower complexity, along with $K = 5$ and $L = 6$ as a tradeoff between complexity and performance. However, due to its limited memory depth, the model is not able to compensate for LTM. Additionally, since the least-squares estimator inherently prioritizes correction of the dominant driven tones, weaker intermodulation products contributing

1350911x, 2026, 1, Downloaded from https://ietresearch.onlinelibrary.wiley.com/doi/10.1049/elt2.70708 by Technische Universität Hamburg Universitätsbibliothek, Wiley Online Library on [14/09/2026]. See the Terms and Conditions (https://onlinelibrary.wiley.com/terms-and-conditions) on Wiley Online Library for rules of use; OA articles are governed by the applicable Creative Commons License

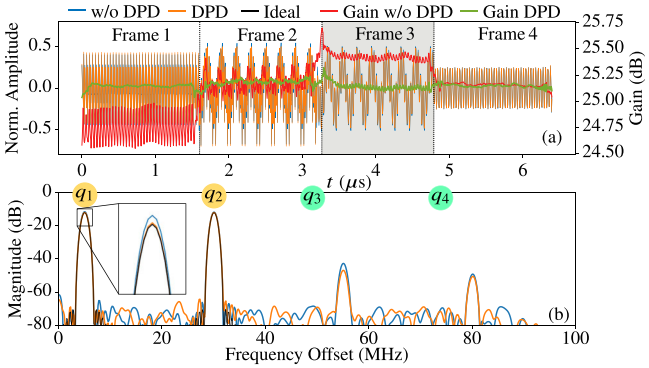


FIGURE 2 | (a) Measured transient signal and gain with and without DPD of the equivalent baseband output signal. (b) Measured spectrum of the signal in frame 3 with and without DPD, with additional illustration of desired qubit excitations (yellow) and idle qubits (green).

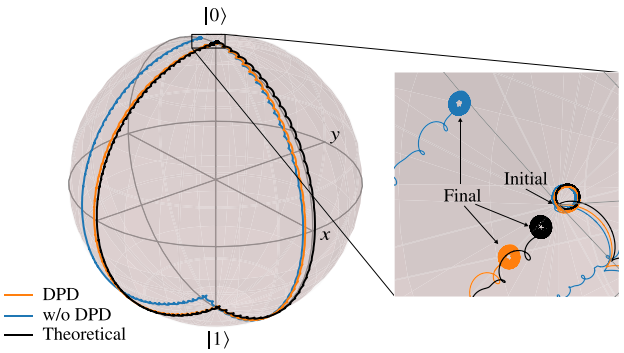


FIGURE 3 | Calculated trajectory of an exemplary sequence (idle, Y_π, $-X_\pi$, idle) within the Bloch sphere, calculated for qubit 1 based on measured control signals.

to the reduced adjacent-channel power ratio (ACPR) improvement are captured less accurately. The absence of cross-terms in the MP structure further limits its ability to model cross-memory interactions between differently delayed tone contributions.

4.2 | Analysis of an Exemplary Sequence

The test signal (pooled across all sequences) has a normalized mean squared error (NMSE) of −17.72 dB and −26.2 dB and an ACPR of −39.13 dB and −41.5 dB, without and with DPD, respectively, where the adjacent channel is defined as the frequency band of the respective idle qubits relative to the driven qubits. The lower ACPR improvement is due to limited model capacity. In the following, the exemplary behavior of qubit 1 in the 15th sequence is analyzed. It consists of an idle period, a Y_π-pulse, a $-X_\pi$-pulse, and a subsequent idle period.

Figure 2a depicts the corresponding transient behavior of the underlying measured in-phase signal part for this sequence, with a PAPR of 6.15 dB, an NMSE of −17.86 dB and −29.25 dB, and an ACPR of −40.03 dB and −41.11 dB, without and with DPD, respectively. The measured gain shows that DPD reduces its variance. The residual transients observed at each frame transition are attributable to STM effects.

Figure 2b depicts the spectrum of frame 3. It reveals that qubit 2 is additionally driven, while qubits 3 and 4 are idling. A magnitude error of 0.76 dB is observed at qubit 1's corresponding tone, which is reduced by DPD to 0.1 dB. Spurious tones occur at 55 MHz and 80 MHz which are slightly reduced by DPD; however, due to their spectral distance from qubits 3 and 4, they do not considerably affect them.

Figure 3 illustrates the simulated state vector trajectory of the exemplary sequence. The trajectory is calculated according to (3). For this, the Hamiltonian (4) is evaluated for the sequence, based on the qubit's equivalent BB signal s_{BB}, which is determined by digitally downconverting the measured signal s'_{IF} to the BB domain of the respective qubit in accordance with its frequency offset and is normalized to the range ±1 for I and Q individually. The first driving pulse within the first sequence is used to determine the static signal phase to initialize the qubit state. The four qubits are considered as four independent single-qubit systems with individual excitation frequencies but subject to the same control signal. According to Figure 3, a qubit phase shift in φ due to LTM is observed with and without DPD, which is not compensated due to limited memory in the chosen model. The oscillations on the state trajectory are caused by the interference from the excitation tones of the other qubits, which is also presented in the theoretical trajectory, which directly derives from x_{IF}. Comparing the final state with the theoretical state, using (5), leads to a fidelity of $F = 99.4$ %. With and without DPD, over-rotation errors accumulate over subsequent pulses, whereas DPD mitigates this effect, resulting in a higher fidelity of $F = 99.81$ % for this exemplary sequence.

4.3 | State-Fidelity Analysis Over Output Power

To generalize the observation, the fidelity is evaluated over a set of output powers. For a decreased average output power P_n, the pulse duration is increased by the same factor to maintain π-pulse generation. The same sequences are executed for each power level and repeated ten times to suppress measurement noise, both without and with DPD applied. The DPD coefficients are recalculated for every output power level.

Figure 4 presents the mean infidelity $1 - F$ for every qubit depending on the relative power level. Even for an ideal PA, the qubit gates would be nonideal due to the interference caused by the excitation signals of the neighboring qubits. Thus, to keep the focus on the fidelity related to nonlinearities and memory effects of the PA, the fidelity with and without DPD is calculated with respect to the theoretical state that results from the signal x_{IF} instead of the ideal state $|\psi_{\mathrm{ideal}}\rangle$. Figure 4 indicates that DPD reduces the infidelity overall. Note that the infidelity without DPD nearly remains constant over the sweep because the linear gain is remeasured each power level step for a fair comparison.

5 | Conclusion

This letter outlines the mitigation of quantum gate errors of microwave-controlled QCs due to nonlinearity and memory effects of the PA in their control signal generators. By

1350911x, 2026, 1, Downloaded from https://ietresearch.onlinelibrary.wiley.com/doi/10.1049/el2.70708 by Technische Universität Hamburg Universitätsbibliothek, Wiley Online Library on [14/09/2026]. See the Terms and Conditions (https://onlinelibrary.wiley.com/terms-and-conditions) on Wiley Online Library for rules of use; OA articles are governed by the applicable Creative Commons License

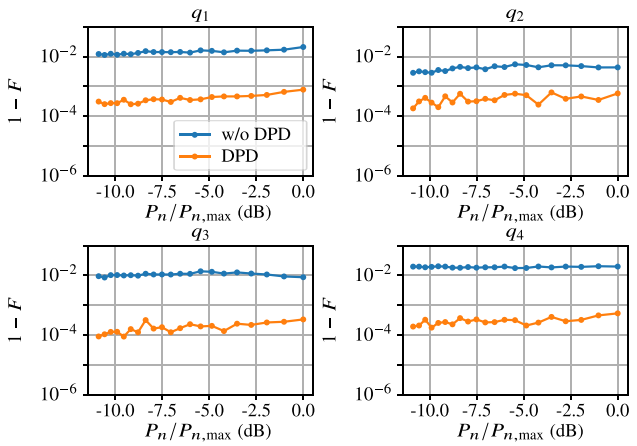


FIGURE 4 | Mean infidelity versus normalized average output power of the different simulated qubits, swept over a set of output powers.

compensating for nonlinear and memory effects using DPD, the accuracy of the control signal can be improved. For this, a feedback loop is introduced to characterize the PA transfer function. Numerical qubit behavior simulations based on measured control signals of a representative signal generation system indicate an improved quantum state fidelity thanks to DPD. Consequently, the application of DPD enables increased processing speeds of QCs without compromising quantum state fidelity, thereby increasing power efficiency.

Author Contributions

Marvin Jaeger: conceptualization, methodology, software, investigation, formal analysis, writing – original draft. **Bartosz Tegowski**: conceptualization, methodology, writing #x02013; review & editing. **Georg Frederik Riemschneider**: conceptualization, writing – review & editing. **Alexander Koelpin**: supervision, funding acquisition, writing – review & editing.

Acknowledgements

This work is part of the Hamburg Quantum Computing (HQC) project, where the required technologies for the implementation of a quantum computer are developed. The project is co-financed by ERDF and Fonds of the Hamburg Ministry of Science, Research, Equalities and Districts (BWFGB).

Open access funding enabled and organized by Projekt DEAL.

Conflicts of Interest

The author declare no conflicts of interest.

Data Availability Statement

The data that support the findings of this study are available from the corresponding author upon reasonable request.

References

1. J. C. Bardin, D. H. Slichter, and D. J. Reilly, "Microwaves in Quantum Computing," *IEEE Journal of Microwaves* 1, no. 1 (2021): 403–427, https://doi.org/10.1109/JMW.2020.3034071.

2. J. C. Bardin, D. Sank, O. Naaman, and E. Jeffrey, "Quantum Computing: An Introduction for Microwave Engineers," *IEEE Microwave Magazine* 21, no. 8 (2020): 24–44, https://doi.org/10.1109/MMM.2020.2993475.

3. J. van Dijk, E. Kawakami, R. Schouten, et al., "Impact of Classical Control Electronics on Qubit Fidelity," *Physical Review Applied* 12 (2019): 044054, https://doi.org/10.1103/PhysRevApplied.12.044054.

4. A. Katz, J. Wood, and D. Chokola, "The Evolution of PA Linearization: From Classic Feedforward and Feedback through Analog and Digital Predistortion," *IEEE Microwave Magazine* 17, no. 2 (2016): 32–40, https://doi.org/10.1109/MMM.2015.2498079.

5. M. Song, S. He, F. You, et al., "A Wideband Analog Linearizer Design Method Based on Frequency-Dependent Gain and Phase Characteristics of Amplifiers," *IEEE Transactions on Microwave Theory and Techniques* 73, no. 10 (2025): 8188–8198, https://doi.org/10.1109/TMTT.2025.3563592.

6. D. Morgan, Z. Ma, J. Kim, M. Zierdt, and J. Pastalan, "A Generalized Memory Polynomial Model for Digital Predistortion of RF Power Amplifiers," *IEEE Transactions on Signal Processing* 54, no. 10 (2006): 3852–3860, https://doi.org/10.1109/TSP.2006.879264.

7. F. M. Ghannouchi and O. Hammi, "Behavioral Modeling and Predistortion," *IEEE Microwave Magazine* 10, no. 7 (2009): 52–64, https://doi.org/10.1109/MMM.2009.934516.

8. D. Wang, M. Aziz, M. Helaoui, and F. M. Ghannouchi, "Augmented Real-Valued Time-Delay Neural Network for Compensation of Distortions and Impairments in Wireless Transmitters," *IEEE Transactions on Neural Networks and Learning Systems* 30, no. 1 (2019): 242–254, https://doi.org/10.1109/TNNLS.2018.2838039.

9. Z. He and F. Tong, "Residual RNN Models with Pruning for Digital Predistortion of RF Power Amplifiers," *IEEE Transactions on Vehicular Technology* 71, no. 9 (2022): 9735–9750, https://doi.org/10.1109/TVT.2022.3182233.

10. Q. Wu, R. Liu, and A. Zhu, "Digital Predistortion Model Extraction Using Reinforcement Learning Without Time-Domain Output Signal Acquisition," *IEEE Transactions on Microwave Theory and Techniques* 73, no. 12 (2025): 10109–10119, https://doi.org/10.1109/TMTT.2025.3598623.

11. P. Krantz, M. Kjaergaard, F. Yan, T. P. Orlando, S. Gustavsson, and W. D. Oliver, "A Quantum Engineer's Guide to Superconducting Qubits," *Applied Physics Reviews* 6, no. 2 (2019): 021318, https://doi.org/10.1063/1.5089550.

12. L. Stefanazzi, K. Treptow, N. Wilcer, et al., "The QICK (Quantum Instrumentation Control Kit): Readout and Control for Qubits and Detectors," *Review of Scientific Instruments* 93 (2022): 044709.

13. M. Jaeger, G. F. Riemschneider, N. Weiß, B. Tegowski, and A. Koelpin, "Design of a Microwave Frontend for a Trapped Ion Quantum Computer," in *Proceedings of the 2025 16th German Microwave Conference (GeMiC)* (IEEE, 2025), 152–155.

14. R. LaPierre, *Introduction to Quantum Computing* (Springer Nature, 2021).

15. R. Jozsa, "Fidelity for Mixed Quantum States," *Journal of Modern Optics* 41, no. 12 (1994): 2315–2323, https://doi.org/10.1080/09500349414552171.

16. A. Khromova, C. Piltz, B. Scharfenberger, et al., "Designer Spin Pseudomolecule Implemented With Trapped Ions in a Magnetic Gradient," *Physical Review Letters* 108 (2012): 220502, https://doi.org/10.1103/PhysRevLett.108.220502.

17. S. Cripps, *RF Power Amplifiers for Wireless Communications*, 2nd ed. (Artech House, 2006).

18. P. N. Landin, S. Gustafsson, C. Fager, and T. Eriksson, "WebLab: A Web-Based Setup for PA Digital Predistortion and Characterization [Application Notes]," in IEEE Microwave Magazine, 16, no. 1 (2015): 138–140, https://doi.org/10.1109/MMM.2014.2367857.

1350911x, 2026, 1, Downloaded from https://ietresearch.onlinelibrary.wiley.com/doi/10.1049/el2.70708 by Technische Universität Hamburg Universitätsbibliothek, Wiley Online Library on [14/09/2026]. See the Terms and Conditions (https://onlinelibrary.wiley.com/terms-and-conditions) on Wiley Online Library for rules of use; OA articles are governed by the applicable Creative Commons License